Materials Horizons

ROYAL SOCIETY OF CHEMISTRY

COMMUNICATION

View Article Online
View Journal | View Issue

Cite this: *Mater. Horiz.*, 2024, 11, 3573

Received 27th February 2024,
Accepted 7th May 2024

DOI: 10.1039/d4mh00211c

rsc.li/materials-horizons

Flexible transparent and hydrophobic SiNCs/PDMS coatings for anti-counterfeiting applications†

Jinfeng Zhang,[a] Yuanfen Huang,[b] Xiaoyuan Zhang,[b] Xin Guo,[a] Kailong Chen,[b] Xiang Feng,[b] Jiajia Kong,[b] Yanqing Liu,[a] Bin Shang,[ab] Weilin Xu[a] and Dongzhi Chen *[ab]

Silicon nanocrystals (SiNCs) have attracted considerable attention in many advanced applications due to silicon's high natural abundance, low toxicity, and impressive optical properties. However, little attention has been paid to fluorescence anti-counterfeiting applications based on lipophilic silicon nanocrystals. Moreover, it is also a challenge to fabricate aging-resistant anti-counterfeiting coatings based on silicon nanocrystals. Herein, this paper presents a demonstration of aging-resistant fluorescent anti-counterfeiting coatings based on red fluorescent silicon nanocrystals. In this work, lipophilic silicon nanocrystals (De-SiNCs) with red fluorescence were prepared first by thermal hydrosilylation between hydrogen-terminated silicon nanocrystals (H-SiNCs) and 1-decene. Subsequently, a new SiNCs/PDMS coating (De-SiNCs/DV) was fabricated by dispersing De-SiNCs into reinforcing PDMS composites with vinyl-capped silicone resin. Interestingly, the De-SiNCs/DV composites exhibit superior transparency (up to 85%) in the visible light range, outstanding fluorescence stabilities with an average lifetime of 20.59 μs under various conditions including acidic/alkaline environments, different organic solvents, high-humidity environments and UV irradiation. Meanwhile, the encapsulation of De-SiNCs is beneficial to enhancing the mechanical properties and thermal stability of De-SiNCs/DV composites. Additionally, the De-SiNCs/DV coating exhibits an excellent anti-counterfeiting effect on cotton fabrics when used as an ink in screen-printing. These findings pave the way for developing innovative flexible multifunctional anti-counterfeiting coatings in the future.

New concepts

Fabricating aging-resistant anti-counterfeiting coatings based on silicon nanocrystals (SiNCs) is a huge challenge. H-SiNCs are easily oxidized when exposed to air and moisture conditions, leading to quenching of photoluminescence. The unstable fluorescence properties greatly limit their potential applications. Therefore, surface modification or passivation of silicon nanocrystals plays a vital role in improving their optical properties. Herein, we present a demonstration of aging-resistant fluorescent anti-counterfeiting coatings based on red fluorescent silicon nanocrystals by a combination of hydrosilylation and polymer encapsulation. To retain the optical transparency of the PDMS matrix, the vinyl-terminated MQ silicone resin is used as a reinforcing agent, which is expected to further enhance the mechanical and wear-resistant properties of the PDMS coating. Meanwhile, new cross-linking networks are further formed by Pt-catalyzed hydrosilylation between the Si–H groups on surfaces of silicon nanocrystals and vinyl groups on MQ silicone resin/PDMS, which hypothetically retard surface migrations of passivated silicon nanocrystals and further stabilize the fluorescence of the composite coating. These findings pave a way for developing innovative flexible transparent coatings and films for anti-counterfeiting and packaging applications based on hydrophobic silicon nanocrystals in the future.

1. Introduction

Science and technology is a double-edged sword. While we enjoy the convenience of an abundance of modern goods that have been made possible by scientific and technological innovations, counterfeiting goods have also flourished on markets, presenting a huge threat to the social community. Thus, various stakeholders such as governments, enterprises, and customers need advanced anti-counterfeiting technologies with robust security features, intelligent multi-level authentication, and sophisticated mechanisms to protect their interests.[1–7] Nowadays, a variety of anti-counterfeiting technologies have emerged, such as watermarks,[8] holograms,[9] metal threads,[10] barcodes,[11] radio frequency identification[12] and so on. Among the existing anti-counterfeiting technologies, fluorescence labeling technology has received considerable attention due to its convenience and low cost. In particular, the pivotal compositions of fluorescent labels are mainly focused on water-borne photoluminescent materials.[13,14] Water-borne photoluminescent materials badly affect service life when encountering water or in a high-humidity environment. Meanwhile, cellulosic substrates with a high hydroxyl content are

[a] State Key Laboratory of New Textile Materials & Advanced Processing Technology, Wuhan Textile University, Wuhan 430200, P. R. China. E-mail: chdozh_2008@163.com
[b] School of Materials Science and Engineering, Wuhan Textile University, Wuhan, 430200, P. R. China

† Electronic supplementary information (ESI) available. See DOI: https://doi.org/10.1039/d4mh00211c

highly hydrophilic and easily degrade when exposed to moisture. Lipophilic anti-counterfeiting materials can effectively prevent water from reacting with photoluminescent materials, thus ensuring the long-term storage of information.[15] Therefore, it is highly desirable to exploit lipophilic anti-counterfeiting materials to develop security labels. However, most of the available photoluminescent materials have their shortcomings. For example, the preparation of organometallic complexes is complex and costly. Organic luminescent materials have many disadvantages such as poor photostability, potential toxicity, cumbersome preparative processes and so forth.[16,17]

Recently, silicon nanocrystals (SiNCs), as emerging nanophotoluminescent materials, have attracted widespread attention in light-emitting diodes,[18] solar cells,[19] anti-counterfeiting, bio-imaging[20,21] and other fields due to their outstanding advantages such as high natural abundance, low cytotoxicity, and excellent optical properties. It is well-known that SiNCs can exhibit fascinating optical phenomena when their size reaches the Bohr scale.[22] However, H-SiNCs are easily oxidized when exposed to air and moisture conditions, leading to quenching of the photoluminescence.[23] The unstable fluorescence properties greatly limit their potential applications. Therefore, surface modification or passivation of silicon nanocrystals plays a vital role in improving the optical properties. To date, varieties of strategies such as thermal hydrosilylation, thiol ligand capping, thiol–ene click chemistry, and polymer encapsulation have been commonly used to protect the surface of H-SiNCs from oxidation and to improve their photoluminescence properties.[24] Among these approaches, thermal hydrosilylation is the most promising strategy for fabricating various desirable functional polymer composites.

Recently, Chen *et al.* prepared near-infrared (NIR) photoluminescent PDMS composites with decyl-terminated silicon nanocrystals (De-SiNCs) fabricated by a combination of hydrosilylation and polymer encapsulation. In particular, the De-SiNCs/PDMS composite exhibits impressive photoluminescence.[25] However, the poor mechanical properties severely retard the anticounterfeiting application of the De-SiNCs/PDMS composite. To date, various reinforcing fillers have been introduced to improve the mechanical properties of PDMS composites including carbon fibers, carbon black, silica, $CaCO_3$, and POSS. However optical transmittance of PDMS composites with reinforcing fillers significantly decreases due to light scattering and absorption. These improvements in mechanical properties are at the cost of optical transmittance of PDMS composites, which is adverse to the photoluminescence of SiNCs/PDMS composites during practical applications.

To address the issues mentioned above, vinyl-capped MQ silicone resin with a low molecular weight (V-MQ) was introduced into the PDMS matrix as a reinforcing agent, which was expected to maintain the high optical transmittance of the original PDMS matrix. At the same time, De-SiNCs were further encapsulated into the PDMS matrix by Pt-catalyzed hydrosilylation. Therefore, the following work is mainly based on the aforementioned hypothesis. Firstly, lipophilic silicon nanocrystals were prepared by thermal hydrosilylation between H-SiNCs and 1-decene, and their optical properties were characterized. Then, De-SiNCs were dispersed into a mixture of V-MQ and V-PDMS (DV), to fabricate a new anti-counterfeiting coating (De-SiNCs/DV coating). Subsequently, different patterns were fabricated by curing the De-SiNCs/DV coating screen-printed on a cotton fabric. Finally, the optical properties and mechanical properties of the De-SiNCs/DV coating were characterized, and the practicability of the De-SiNCs/DV coating for anti-counterfeiting applications was examined and discussed.

2. Experimental section

2.1. Materials

SiO (300 mesh) was obtained from Beijing Huangqiu Jinxin International Technology Co., Ltd (Beijing, China). 1-Decene (De) was purchased from Aladdin Bio-Chem Technology Co. Ltd ($\geq$99.0%, Shanghai, China). Absolute ethanol, *n*-hexane, petroleum ether (30–60 °C), and hydrofluoric acid (40%) were supplied from Sinopharm Chemical Reagent Co., Ltd (Shanghai, China). Vinyl terminated polydimethylsiloxane (V-PDMS) [viscosity, 10 000 cSt, vinyl content, 0.25 wt%], and polymethylhydrogenosiloxane (PMHS, viscosity, 50 cSt, hydrogen content: 0.5 wt%) were kindly provided by Shandong Dayi chemical co., Ltd. Vinyl terminated MQ silicone resin (V-MQ) [the molar ratio of M to Q is 1.1 : 1, viscosity, 750 cSt] and Karstedt catalysis (platinum divinyl tetramethyl disiloxane complex) were prepared in our laboratory. The structure and molecular weight characterization of the synthesized MQ are shown in Fig. S1–S4 (ESI†).

2.2. Synthesis of the De-SiNCs

De-SiNCs were prepared according to the literature method.[26,27] The detailed procedure is described as follows: 0.15 g of the SiO powder was ground for around 1 h before being transferred to a plastic beaker, and then absolute ethanol (10 mL) and HF (40%, 20 mL) were added to the plastic beaker, respectively (personnel should be well-trained in the handling of HF). The H-SiNCs were liberated from the silicon-oxide powder by HF etching for 6 h in a fumed hood with stirring. Then, the resultant H-SiNCs were extracted from the aqueous solution by petroleum ether (30–60 °C, 25 mL). The extracted dispersion of H-SiNCs was transferred into a Teflon-lined autoclave (100 mL capacity), and 1-decene (10 mL) was added into the Teflon autoclave. The mixture was ultrasonically dispersed for 5 min. Then the mixture was purged with highly pure argon three times. Finally, the Teflon autoclave was sealed and placed in an oven at 170 °C for 6 h. The synthetic procedures are described in Scheme 1a.

After the reaction, the resultant De-SiNCs were collected by centrifugation at 8000 rpm for 5 min in an ambient environment. The precipitate was taken out and washed three times using methanol and *n*-hexane as polar and antipolar solvents (volume ratio: 1 : 3), respectively, until the supernatant could not emit fluorescence under a UV lamp. Finally, the collected precipitate was dried in a vacuum oven to afford the purified De-SiNCs for the following experiment.

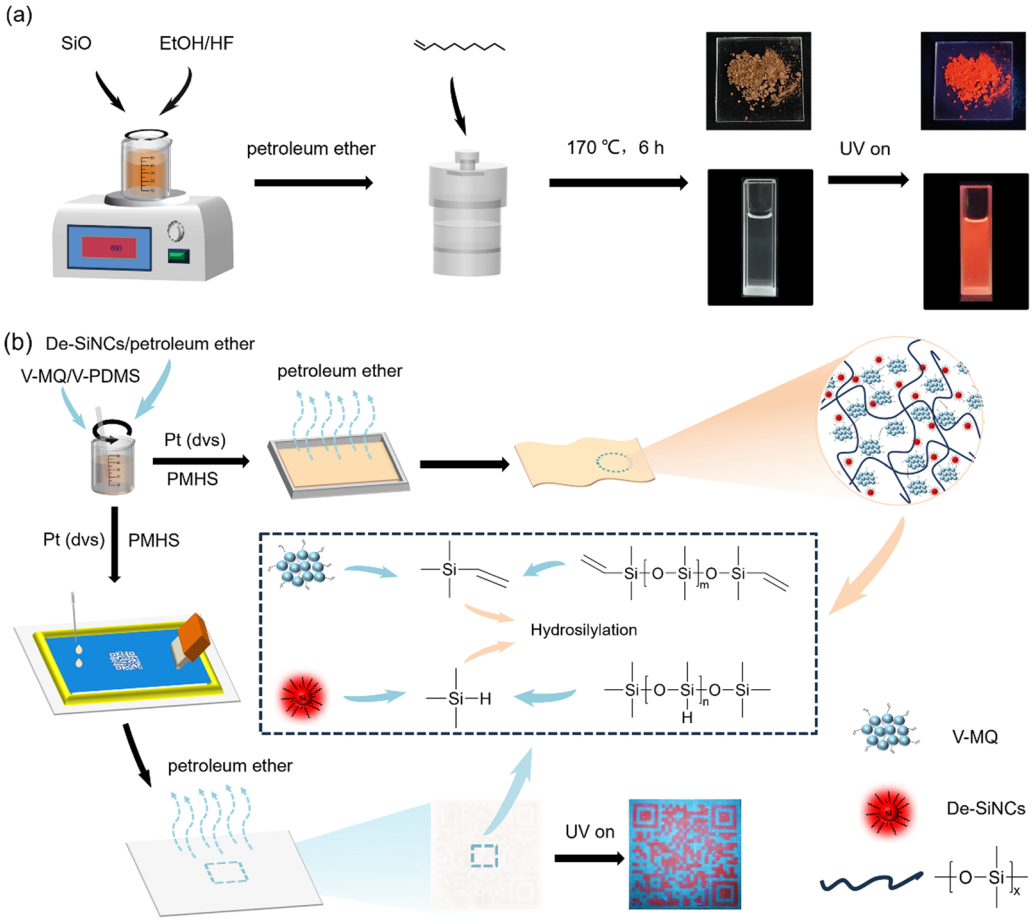

Scheme 1 (a) Schematic diagrams of the synthetic process of De-SiNCs, and (b) preparation of De-SiNCs/DV sheets and fabric labels.

2.3. Preparation of the De-SiNCs/DV coating

V-PDMS and V-MQ were mixed in a mass ratio of 1 : 0.03 by mass, by mechanically stirring at a speed of 230 rpm for 3 h. After mixing, a colorless and transparent fluid (DV fluid) was obtained. Then, desirable amounts of Pt catalyst, PMHS and De-SiNCs (mass fractions of 0.1, 0.3, 0.5, 0.7, and 1.0 wt%) were added to a certain amount of DV fluid with mechanical stirring for 10 min, respectively. After stirring, the De-SiNCs/DV coating was obtained by removal of low volatiles under vacuum at room temperature for 30 min. Detailed formulations of De-SiNC coatings are listed in Table 1.

Table 1 Detailed formulation of De-SiNCs/DV coatings

Sample	DV (g)	Pt-Karatedt catalysis (μL)	PMHS (g)	Dispersion of De-SiNCs (g)	Weight percentage of De-SiNCs (g)
0	2.5	6	0.25	0	0
0.1	2.5	6	0.25	0.25	0.1
0.3	2.5	6	0.25	0.75	0.3
0.5	2.5	6	0.25	1.25	0.5
0.7	2.5	6	0.25	1.75	0.7
1.0	2.5	6	0.25	2.50	1.0

2.4. Fabrication of De-SiNCs/DV sheets and fabric labels

The De-SiNCs/DV coating was dripped on the acrylic plate and cured at 100 °C for 1 h. Similarly, different customized patterns were screen-printed on a cotton fabric that was cured at 100 °C for 1 h, as shown in Scheme 1b.

2.5. Characterization

Th high resolution transmission electron microscopy (HRTEM) image of De-SiNCs was acquired with an FEI Talos F200X at an accelerating voltage of 200 kV. Fourier-transform infrared (FTIR) spectra (4000–500 cm^{-1}) of specimens were recorded using a Nicolet 5700 FT-IR spectrometer (Thermo Electron Corporation, Waltham, MA). X-ray diffraction (XRD) patterns of De-SiNCs were recorded on an UItima IVX-ray diffractometer (Rigaku Corporation) using Cu Ka radiation, and the step size and scanning rate were 0.02° and 5° min^{-1}, respectively. The X-ray photoelectron spectroscopy (XPS) spectrum of De-SiNCs was obtained using a Thermo Scientific system (K-Alpha, USA) with a scanning X-ray photoelectron spectrometer microprobe. UV-Vis absorption spectra of liquid and solid specimens were recorded using a UV-2700 UV-Vis spectrophotometer (Shimadzu Company). The fluorescence spectra of specimens were recorded using an F-4700 fluorescence spectrophotometer (Hitachi, Japan) with a xenon lamp as the source of excitation.

The absolute photoluminescence quantum yield of coatings was measured using an FLS-1000 spectrophotometer with an integrating sphere (Edinburgh, UK). The optical measurements required for the experiment were all operated at room temperature under ambient conditions. All photos and videos were taken using a smartphone. Thermogravimetric analysis (TGA) was performed on a TG 209F1(NETZSCH Instruments) under a gas flow of 50 mL min^{-1}. About 10 mg of sample cut as small pieces was heated in a platinum crucible in a nitrogen atmosphere from ambient temperature to 800 °C at a constant rise of temperature (10 °C min^{-1}). Mechanical tensile tests were performed on a universal testing machine (Instron 8871, UK, capacity 25 kN) at 25 °C. The tensile strength, elongation at break, and modulus were measured using a crosshead speed of 10 mm min^{-1}. The tensile stress–strain test of each coating was performed according to the GB/T 528-2009 standard. The adhesion test of each coating was carried out according to the GB/T 7124-2008 standard. Dynamic mechanical analysis (DMA) was carried out on a Q800 DMA analyzer (TA Instruments, USA) in the dual-cantilever bending mode with a specimen size of 50 mm × 16 mm × 3 mm. For each measurement, at least three specimens were tested under the same conditions.

3. Results and discussion

3.1. Preparation and characterization of De-SiNCs

During the chemical etching process, HF continuously removed surface silicon-oxide species, and H-SiNCs are liberated. However, H-SiNCs are easily corroded when exposed to air or water. To prevent them from corroding, 1-decene is used as a ligand to passivate the surface of H-SiNCs by thermal hydrosilylation, as shown in Fig. 1a. The TEM image shows that the De-SiNCs appear in the form of monodispersed spherical particles, as observed in Fig. 1b. The inset in Fig. 1b exhibits that the resultant De-SiNCs have an average size of 2.90 ± 0.03 nm, which is in good agreement with the results of SiNCs reported in previous literature.[28,29] Meanwhile, DLS analysis shows that the diameter of the De-SiNCs dispersed in petroleum ether (5.53 ± 1.15 nm) is larger than that of the TEM result as shown in Fig. S5 (ESI†), which is attributed to the interaction between the solvent and the surface ligand.[30] The HRTEM image reveals that the spherical De-SiNCs have a discernible lattice fringe spacing of 0.31 nm, which matches with the *d*-spacing of the (111) plane of the diamond cubic lattice of Si,[26] as shown in Fig. 1c.

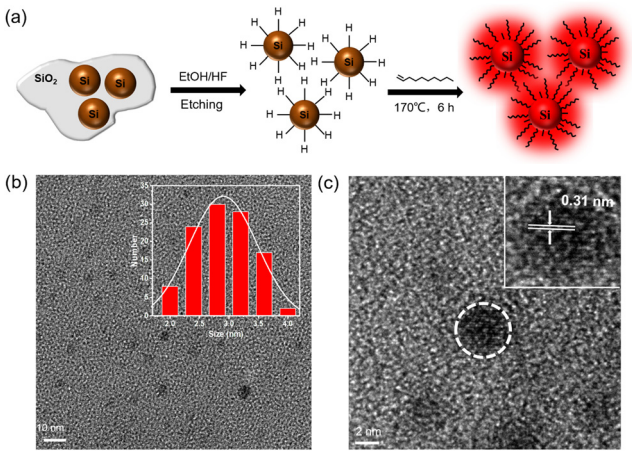

Fig. 1 (a) Schematic diagram of the preparative process of De-SiNCs. (b) TEM image of De-SiNCs. The inset is the size distribution of SiNCs determined based on the statistical analysis of over 30 dots in the TEM image. (c) HRTEM image of De-SiNCs. The inset is the magnified region circled with the white dashed-line domain.

To gain insight into the surface composition, the FTIR spectra of SiO, 1-decene and De-SiNCs were recorded, respectively. As shown in Fig. 2a, compared to those of the starting materials including SiO and 1-decene, the characteristic absorption bands located at 2850–2922 and 1456, 1056, and 796 cm^{-1} are attributed to the stretching and deformation vibrations of C–H, the Si–O–Si and Si–C stretching vibrations, respectively, confirming that 1-decene is successfully covalently bound to the surface of H-SiNCs *via* thermal hydrosilylation, which was consistent with previous reports.[31] Notably, a small peak at 2092 cm^{-1} is attributed to the Si–H stretching vibration, indicating that the surfaces of silicon nanocrystals were partly passivated by 1-decene.[32] Moreover, a broad absorption band at 3500 and a small peak at 932 cm^{-1} are assigned to the stretching vibration of Si–OH and the asymmetric deformative vibration of Si–H, respectively. In this case, Si–OH stems from the adventitious oxidation of Si–H on the surface of De-SiNCs in ambient air. As displayed in Fig. 2b, XRD patterns of the De-SiNCs and SiO show a similar broad diffraction angle centered at about 21°, which is attributed to the diffraction feature of amorphous SiO_2. Additionally, some discernible diffraction angles located at 28, 47, and 56° are indexed to the (111), (220), and (311) planes of the diamond cubic lattice of silicon, respectively, proving that De-SiNCs are present in the diamond cubic structure.[33]

XPS spectroscopy was employed to further characterize the surface chemical compositions of the De-SiNCs. The full XPS survey spectrum of the resultant De-SiNCs demonstrates that four elements of O, C, Si, and F with atomic percentages of 33.98%, 18.03%, 27.45%, and 4.34% are observed in Fig. 2c. Meanwhile, the EDS mapping of De-SiNCs further verifies that the De-SiNCs are composed of mainly O, Si, C and F elements, as shown in Fig. S6 (ESI†). The corresponding peaks of O 1s, C 1s, Si 2s, Si 2p, and F 1s are located at 532.78, 284.54, 154.49, 104.51, and 687.82 eV, respectively. Subsequently, the high-resolution spectrum of O 1s (Fig. 2d) is deconvoluted into a major peak at 532.78 eV, which is attributed to the Si–O group.[34] The fitting peak also demonstrates the presence of oxygen-containing groups, as confirmed by FTIR. Fig. 2e presents the C 1s spectrum of De-SiNCs that is deconvoluted into two peaks at 286.43 and 284.79 eV, attributed to C–Si and C–C, respectively,[34] confirming that 1-decene is successfully bound onto the surface of H-SiNCs by thermal hydrosilylation. Meanwhile, the Si 2p spectrum of De-SiNCs is fitted into four peaks at 104.18, 103.88, 100.78 and 99.18 eV, which are attributed to Si–O–Si, Si–OH, Si–C and Si–Si,[26,35] respectively, as shown in

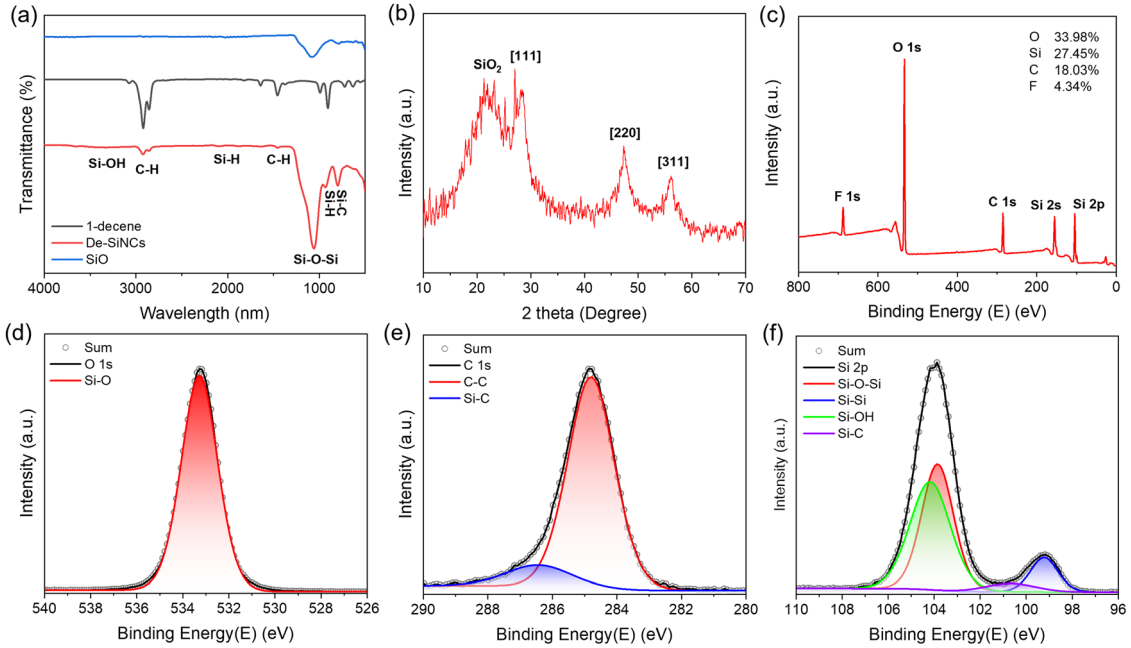

Fig. 2 (a) FTIR spectra of SiO, 1-decene and De-SiNCs. (b) XRD patterns of De-SiNCs. (c) XPS survey spectrum of De-SiNCs, and (d)–(f) the corresponding high-resolution XPS fitting results for the O 1s, C 1s, and Si 2p spectra of De-SiNCs.

Fig. 2f. Collectively, H-SiNCs are successfully passivated with 1-decene by thermal hydrosilylation.

3.2. Optical properties of the De-SiNCs

The photos of the resultant colloidal dispersion of the De-SiNCs are shown in Fig. 3a. Under daylight, the colloidal dispersion of the De-SiNCs is present in a clear and transparent solution, indicating that the De-SiNCs were uniformly dispersed, while the De-SiNCs can emit bright red fluorescence under UV lamp (254/365 nm) irradiation. To gain insight into the optical properties of De-SiNCs, their UV-Vis absorption and PL spectra were recorded. Fig. 3b clearly shows that De-SiNCs have almost no observable absorbance at 400–800 nm, which is attributed to the indirect bandgap transition of silicon. Significantly, the absorption bands can be seen at 200–400 nm. In particular, a distinct absorption peak at 207 nm and a broad peak at 280 nm in the UV-Vis absorption spectrum are observed, which should be attributed to the intrinsic direct bandgap transition of the silicon core and the Γ point, respectively.[26,32,36] As shown in Fig. 3c, the PL emission spectra of the De-SiNCs distinctly exhibit the emission maximum shifts from 613 nm to 633 nm with an increase in the excitation wavelength from 250 to 370 nm, implicating the excitation-dependent properties of the De-SiNCs. The CIE 1931 diagram in Fig. 3d shows that the color coordinates of the De-SiNCs show a clear redshift in color with an increase in the excited wavelength. To evaluate storage stability, the zeta potential of the resultant De-SiNCs was measured. Fig. 3e presents the zeta potential of the De-SiNCs dispersed in petroleum ether, which is -32.93 ± 0.36 mV, indicating the presence of some negatively charged hydroxyl groups on the surface of silicon. It is emphasized that the negative electrostatic repulsion between the De-SiNCs imparts the dispersion of the De-SiNCs in petroleum ether with excellent colloidal stability.[37]

To examine their storage stability, the particle size and surface potential of the De-SiNCs before and after storage for 7 days are shown in Fig. S7 (ESI†), which shows no significant change in particle size and surface potential of De-SiNCs before and after storage for 7 days. In addition, the pH fluorescence stability of De-SiNCs was also examined. Fig. 3f presents that dispersion of the De-SiNCs has better fluorescence stability in acidic and neutral environments. With an increase in the pH value, the fluorescence intensity of the De-SiNCs monotonously decreases, and no shift in the PL emission maximum can be observed. It is reasonable that under alkaline conditions, a large amount of OH^- captures H from the Si–H bonds on the surface of De-SiNCs, leading to the corrosion of the silicon surface.[38] The surface corrosion results in a decrease in the luminescence efficiency of the De-SiNCs.

As shown in Fig. 3g, the polarity of different organic solvents cannot change the maximum emission of De-SiNCs. However, there are obvious differences in the intensity of the emission peak of the De-SiNCs, which is attributed to the dispersibility in different organic solvents. Fig. 3h shows that the fluorescence intensity of De-SiNCs gradually decreases with an increase in time, which should be attributed to water corrosion of De-SiNCs under the 90% humidity environment. Similarly, the fluorescence intensity of the De-SiNCs gradually decreases with an increase in the UV irradiation time, as shown in Fig. 3i. The decreasing intensity is attributed to the formation of dangling bonds on the De-SiNCs by photocleavage and adventitious oxidation in air.[27]

3.3. Fabrication, optical properties and water-repellency of De-SiNCs/DV films

Obviously, after curing, the disappearance of vinyl groups (3060 and 1598 cm^{-1}) from V-MQ and Si–H groups (2152 cm^{-1}) from PMHS corroborates that cross-linking De-SiNCs/DV films were

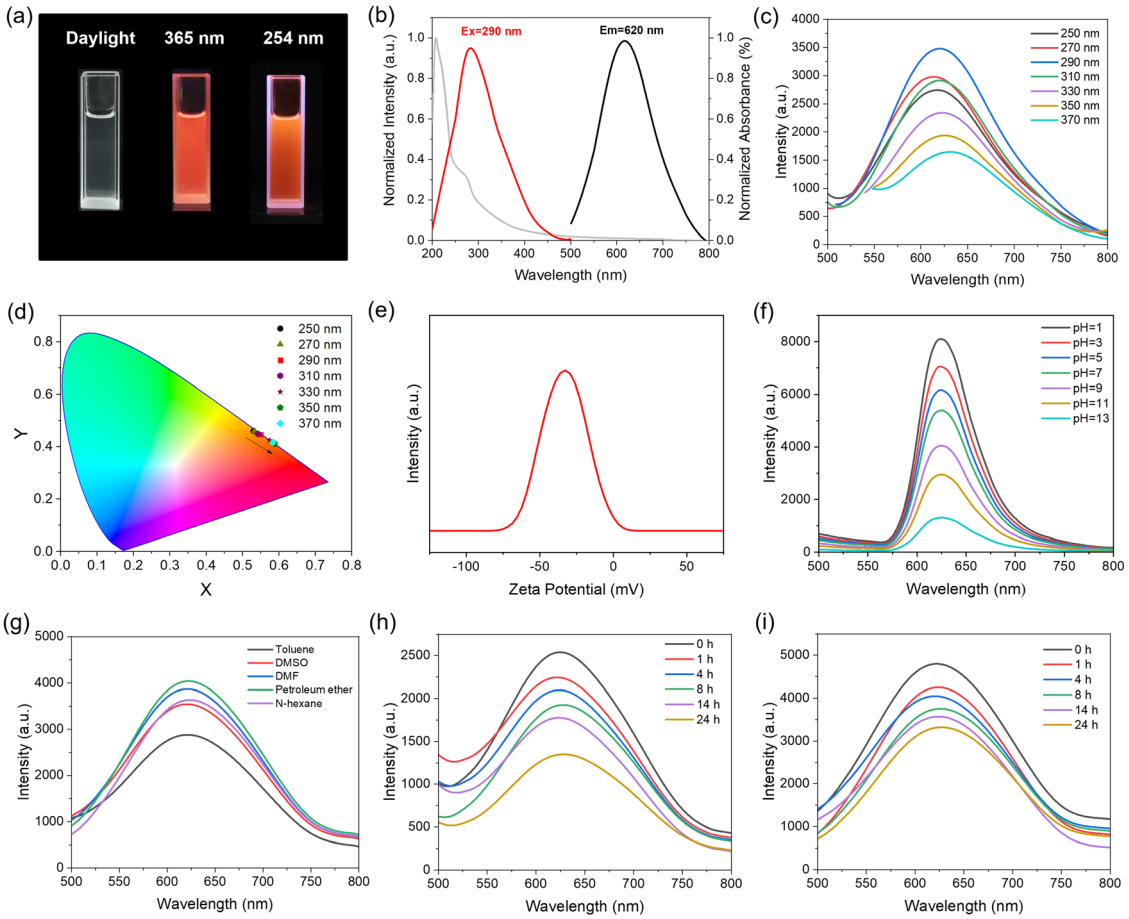

Fig. 3 (a) Photos of the as-prepared De-SiNCs dispersed in petroleum ether under daylight and UV lights (365/254 nm). (b) Normalized UV-Vis absorption, PL excitation, and emission spectra. (c) The PL emission spectra under the varying excitation wavelengths ranging from 250 to 370 nm. (d) CIE 1931 chromaticity diagram for the photoluminescent color coordinates of the dispersions of De-SiNCs under irradiation of changeable wavelengths. (e) Zeta potential of the aqueous dispersion for the resultant De-SiNCs in petroleum ether. (f) Fluorescence stability of De-SiNCs under different pH conditions. (g) Fluorescence intensity of the De-SiNCs dispersed in different organic solvents. The fluorescence intensity of the De-SiNCs powder (h) in a 90% humidity environment and (i) UV light irradiation for variable times.

successfully fabricated by Pt-catalyzed hydrosilylation, as shown in Fig. 4a. At the same time, the color of De-SiNCs/DV films becomes dark with the mass fraction of De-SiNCs after curing, as shown in photographs in Fig. 4b. It is noteworthy that the fluorescence intensity of the De-SiNCs/DV film becomes stronger when the mass fraction of De-SiNCs increases to 0.5%. However, it begins to become weaker when the weight fraction of De-SiNCs continuously increases from 0.5% to 1.0% as displayed in Fig. 4c. The decreasing fluorescence intensity of the De-SiNCs/DV films should be attributed to the synergistic effect of light scattering and transmittance. The increasing amount of the De-SiNCs would result in strong light scattering and low transmittance of the De-SiNCs/DV films. As a result, the limited light energy at a wavelength of 290 nm cannot efficiently excite the De-SiNCs/DV films.

As shown in Fig. 4d, the De-SiNCs/DV films exhibit lowering transmittance with the loading of De-SiNCs from the UV region to the visible region. Most notably, the transmittance of the De-SiNCs/DV film is above 85% in the wavelength range of 500 nm to 800 nm, as shown in Fig. 4e. Significantly, the transmittance of the composite film with 0.5% De-SiNCs can reach more than 90%. The high transmittance can be attributed to the organic/inorganic hybridized nanophases, which prevent light scattering caused by phase separation. Afterwards, the hydrophobic properties of the De-SiNCs/DV films were assessed by static water contact angle (WCA) measurements. As shown in Fig. 4f, the WCA values of the De-SiNCs/DV films with De-SiNCs are much higher than that of the composite film without De-SiNCs. The hydrophobicity of the De-SiNCs/DV film is attributed to the synergistic effect between the low-surface-energy PDMS matrix and the oleophilic De-SiNCs. Importantly, the composite film with 0.5% De-SiNCs exhibits the maximum WCA of 125°, indicating excellent water-repellence. Therefore, the De-SiNCs/DV film with 0.5% De-SiNCs was used for the following applications.

To gain insight into the optical properties of the De-SiNCs/DV film, its UV-Vis absorption and PL spectra were recorded, respectively. Obviously, a hypochromic shift (20 nm) in the PL excitation maximum is found as compared to that of the De-SiNC dispersion, as shown in Fig. 5a and 3b. The striking blue-shift phenomenon should be attributed to the synergistic effect of adventitious oxidation on the surfaces of the De-SiNCs, and

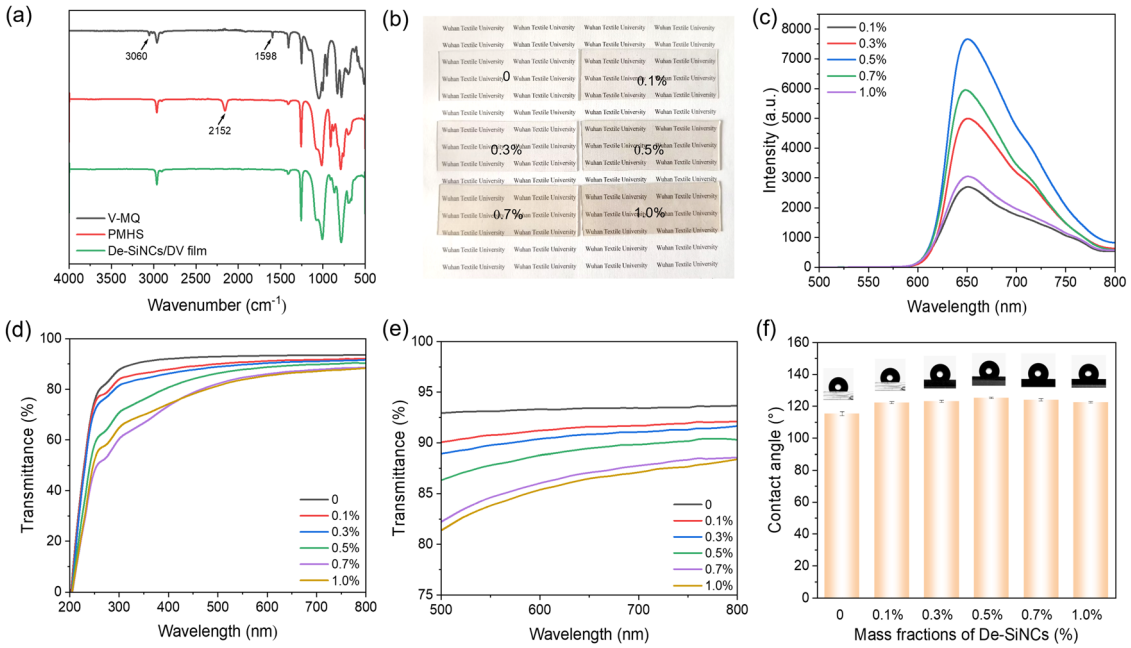

Fig. 4 (a) FTIR spectra of V-MQ, PMHS and the De-SiNCs/DV film. (b) Photos of De-SiNCs/DV films with different mass fractions of De-SiNCs. (c) The PL emission spectra of De-SiNCs/DV films at an excitation wavelength of 290 nm. (d) Transmittance spectra of De-SiNCs/DV films. (e) Enlarged transmittance spectra in the wavelength range of 500 nm to 800 nm. (f) Static water contact angle of De-SiNCs/DV films with different mass fractions of De-SiNCs.

the restriction of the cross-linking PDMS chains. Meanwhile, a pronounced bathochromic shift (30 nm) in the PL emission maximum is observed, compared to that of the De-SiNC dispersion. The red-shift phenomenon in PL emission maximum could be due to further passivation resulting from Pt-catalyzed hydrosilylation between De-SiNCs and PDMS. As shown in Fig. 5b, the PL emission spectra of the De-SiNCs distinctly exhibit an unchanged emission maximum located at about 650 nm with an increase in the excitation wavelength from 240 to 300 nm, implicating excitation-independent property for

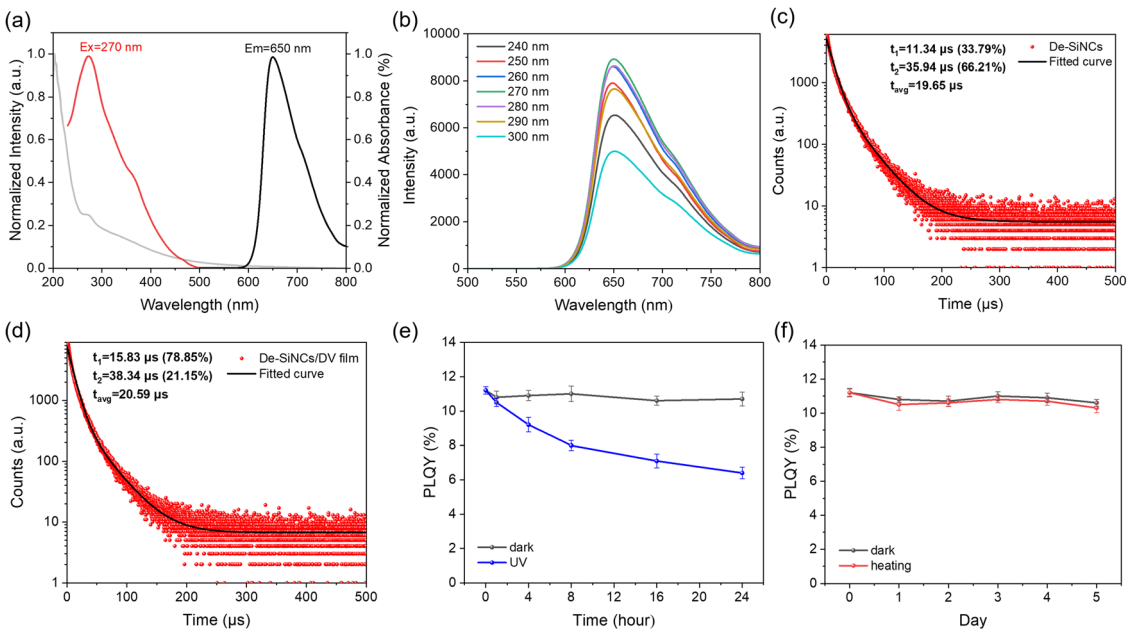

Fig. 5 (a) Normalized UV-Vis absorption, PL excitation, and emission spectra of the De-SiNCs/DV film. (b) The PL emission spectra of the De-SiNCs/DV film excited at variable wavelengths ranging from 240 nm to 300 nm. (c) Time-resolved PL decay curves of the dispersion of the De-SiNCs. (d) Time-resolved PL decay curves of the De-SiNCs/DV film. (e) PL quantum yield of the De-SiNCs/DV films irradiated with UV light and stored under dark conditions for variable times. (f) PL quantum yield of the De-SiNCs/DV films immersed in 80 °C water and stored under dark conditions for variable times.

the De-SiNCs/DV film. Subsequently, the fluorescence lifetime of the De-SiNCs and the De-SiNCs/DV film was determined by measuring the PL decay at the emission maximum. As shown in Fig. 5c and d, the fluorescence decay cures can be fitted using a biexponential function, indicating dual emission channels in both the De-SiNCs and the De-SiNCs/DV film. Interestingly, the average lifetime of the De-SiNCs/DV film was calculated to be 20.59 μs, which is higher than 19.65 μs for the De-SiNCs dispersion. The increasing fluorescence lifetime indicates that the fluorescence stability of the De-SiNCs was further enhanced by Pt-catalyzed hydrosilylation and polymer encapsulation.

To further evaluate the fluorescence stability, the De-SiNCs/DV films were subjected to hydrothermal treatment at 80 °C and UV irradiation, and the PL quantum yield of the De-SiNCs/DV films was recorded. As shown in Fig. 5e, the quantum yield of the De-SiNCs/DV film gradually decreases with an increase in the UV irradiation time. As compared with the reference sample with dark conditions, the quantum yield of the De-SiNCs/DV films decreases by 50% when the UV irradiation time reaches 24 h. The decreasing PL quantum yield is attributed to dangling bond formation on the De-SiNCs by photocleavage,[27] and adventitious oxidation in air. Additionally, the De-SiNCs/DV films were treated with hot water at 80 °C for several days, and their absolute PL quantum yield was also determined. To avoid interference of daylight, the De-SiNCs/DV film was also stored under dark conditions for the same time intervals, the absolute PL quantum yield was also determined as a reference. Most notably, comparing the reference, the absolute PLQY of the De-SiNCs/DV film is about 10.3%, remaining unchangeable with an increase in the immersion time, corroborating that the De-SiNCs/DV film has excellent fluorescence stability even in high-humidity environments.

As shown in Fig. 6a, both the pure DV composite film and the De-SiNCs/DV film show good resistance to the organic solvents. Toluene, tetrahydrofuran, and petroleum ether have a significant swelling effect on both the DV film and the De-SiNCs/DV film, but the residual mass of the film remains above 95% after solvent swelling. The solvent resistance of the De-SiNCs/DV film is attributed to the successful cross-linking and the invading prevention effect of the V-PDMS.[39] Interestingly, the De-SiNCs/DV film retains excellent fluorescence stability after being immersed in different organic solvents for 24 h, as shown in Fig. S8 (ESI†). The De-SiNCs/DV film impregnated in toluene shows blue fluorescence under a UV lamp, which recovers to the original red fluorescence after toluene evaporation.

To determine water absorption (WA), the cured DV film and De-SiNCs/DV film were placed in an environment with 90% humidity at different times, respectively. As shown in Fig. 6b, the WA mass of the DV film and De-SiNCs/DV film gradually increases with time, and finally achieves equilibration after exposure to moisture for 4.5 h. The WA of the DV film is 0.93% because of the intrinsic hydrophobic property of PDMS. When De-SiNCs (0.5%) were added, the WA of the De-SiNCs/DV film further decreased to 0.37% implying that the addition of De-SiNCs is beneficial for lowering the WA of the De-SiNCs/DV film.

3.4. Mechanical properties and thermal behavior of the De-SiNCs/DV films

Subsequently, the mechanical properties of De-SiNCs/DV film were examined, such as bonding strength and tensile properties.

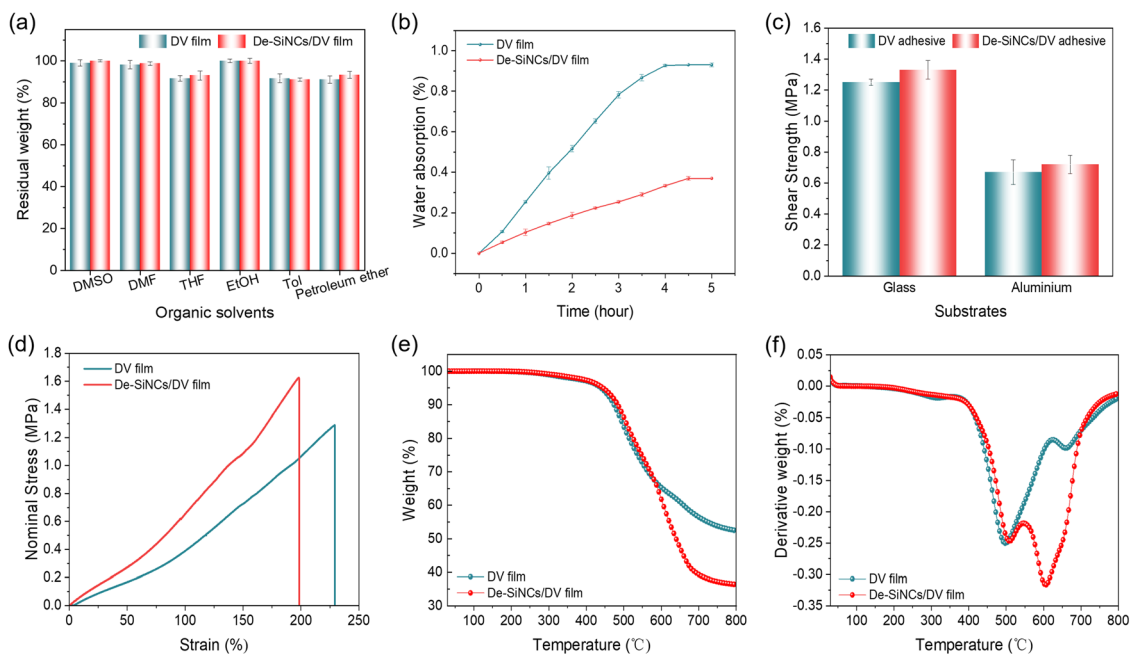

Fig. 6 Properties of De-SiNCs/DV films. (a) Solvent resistance test of the DV film and De-SiNCs/DV film (residue weights of the film after soaking in different solvents for 24 h). (b) Water absorption of the DV film and De-SiNCs/DV film in 90% humidity for different times. (c) The adhesion of the uncured DV and the De-SiNCs/DV as the adhesive. (d) Stress–strain curve of the DV film and De-SiNCs/DV film. TGA curves (e) and DTG curves (f) of the DV film and De-SiNCs/DV film in a nitrogen atmosphere.

To assess bonding strength, the uncured DV and the De-SiNCs/DV have been used as adhesives for glass and aluminum sheets. As shown in Fig. 6c, the adhesion of the DV film and De-SiNCs/DV film on aluminium plates is only 0.67 ± 0.08 MPa and 0.72 ± 0.06 MPa, respectively. However, the adhesion of the DV film and De-SiNCs/DV film on glass sheets can reach 1.25 ± 0.02 MPa and 1.33 ± 0.06 MPa, respectively. Due to the existence of Si–OH groups on the glass surface, plentiful Si–O–Si groups are formed by Pt-catalyzed polycondensation during the curing process, leading to high bonding strength to glass sheets as compared to aluminum plates.[40] Fig. 6d shows the stress–strain curves of the DV film and the De-SiNCs/DV film. It is clearly found that the tensile strength and Young's modulus of the De-SiNCs/DV film increases by 25% (1.62 ± 0.02 MPa) and 50% (1.21 ± 0.01 MPa), respectively, compared to those of the DV film, confirming that incorporation of De-SiNCs improves the mechanical properties of PDMS composites, as shown in Fig. 6d and Fig. S9 (ESI†). The reinforced mechanical properties of the De-SiNCs/DV film are ascribed to the cross-linking three-dimensional networks among V-PDMS chains, V-MQ and De-SiNCs.[25,41] As shown in Fig. S10 (ESI†), the storage modulus of the De-SiNCs/DV film is larger than that of the DV film at room temperature, which corresponds to the results of the tensile testing of the De-SiNCs/DV films. As the temperature decreases, the storage modulus of the De-SiNCs/DV film is lower than that of the DV film. In addition, the addition of De-SiNCs has no significant impact on the glass transition temperature of the PDMS materials, which remains around −120 °C.[42]

Additionally, the thermal behavior of De-SiNCs/DV films was evaluated by TGA under a nitrogen atmosphere, as shown in Fig. 6e and f. Obviously, all the PDMS composites have two degradative steps in thermal degradation. The De-SiNCs/DV film has higher decomposition temperatures than the DV film when they lost the same weight percent of the initial mass at less than 580 °C. During the whole degradation, the temperature at the first maximum

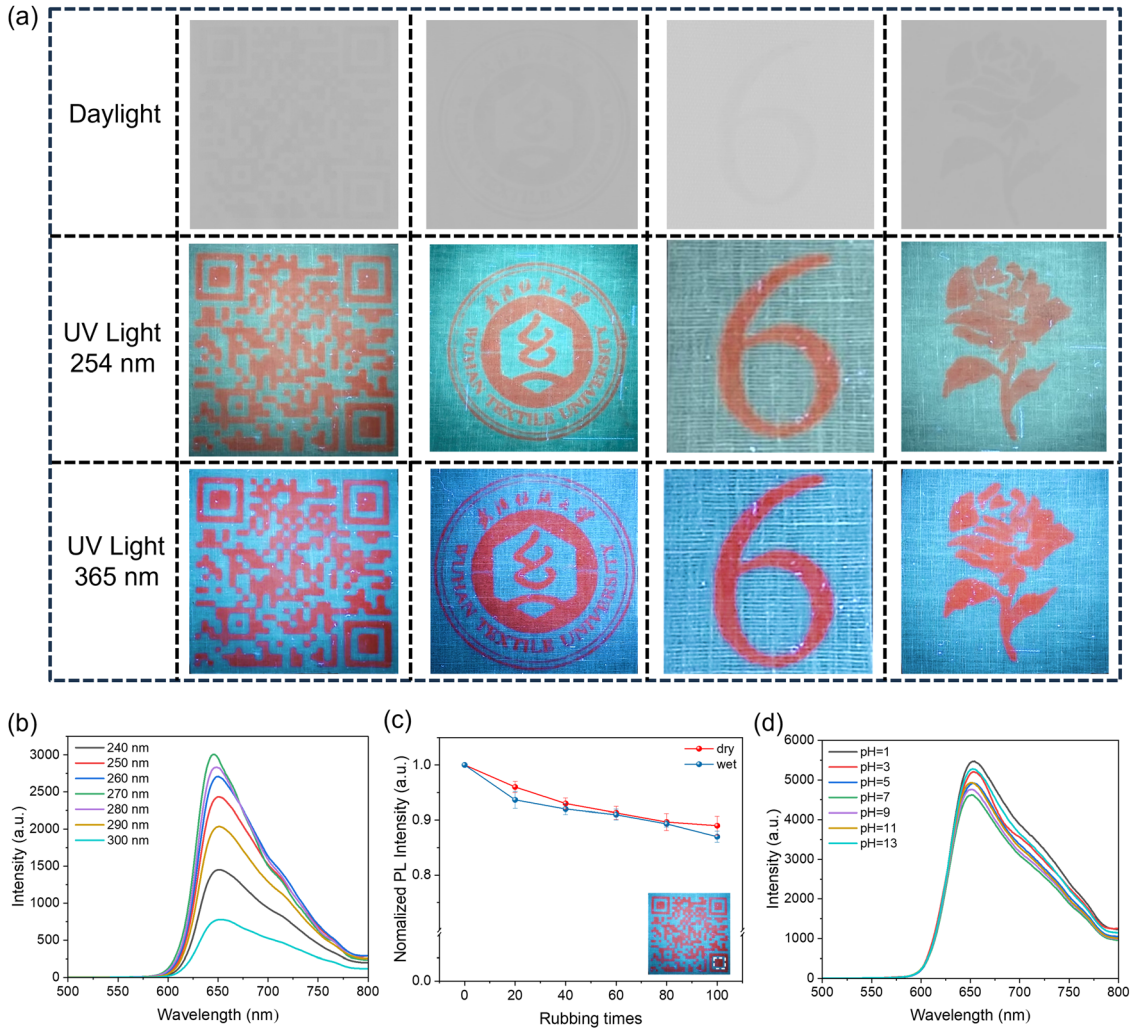

Fig. 7 (a) Photographs of the customized labels including campus QR codes, the campus logo, the number "6" and the rose screen-printed on cotton fabrics using the De-SiNCs/DV composite as the coating. (b) The PL emission spectra of the De-SiNCs/DV coating on cotton fabric at the excitation wavelength ranging from 240 to 300 nm at room temperature. (c) Wet and dry fastness of the De-SiNCs/DV coating printed on cotton fabrics. The inset is a photo of the fabric label with campus QR codes printed on cotton fabric under 365 nm irradiation, the white dashed square is the rubbed area for measurements. (d) Fluorescence response of the De-SiNCs/DV coating to different pH values. The printed QR codes were immersed in different pH solutions for 24 h, and the fluorescence intensity was measured after drying at room temperature.

degradation rate was delayed from 495 °C to 510 °C as the De-SiNCs were added into the PDMS matrix. The delayed degradation temperature is ascribed to entanglement interactions between PDMS chains and hydrocarbon chains capped on the surface of De-SiNCs.[41] However, the residual yield of the De-SiNCs/DV film at 800 °C decreased to 36.4%, which is lower than that of the DV composite (52.5%). The decreasing residual yield should be ascribed to fewer 3D cross-links as compared with the DV film because the De-SiNCs took part in Pt-catalysed hydrosilylation during the curing process. The degradation activation energies of the De-SiNCs/DV films at a heating rate of 10 °C min^{-1} are also calculated by Van Krevelan's method.[43,44] It is found that the degradation activation energy increases from 45.97 kJ mol^{-1} for the DV film to 97.63 kJ mol^{-1} for the De-SiNCs/DV film, as shown in Table S1 (ESI†). The increasing degradation activation energy indicated the strong interaction between PDMS chains and nano–micro particles.[41] These results further demonstrate that adding De-SiNCs is beneficial for improving the thermal stability of the PDMS composites.

3.5. Anti-counterfeiting applications of De-SiNCs/DV coatings

To examine the practicability of the De-SiNCs/DV coatings, the campus QR codes, school logo, the number "6" and the rose are printed on cotton fabrics using the De-SiNCs/DV coatings, respectively. The patterns on fabric labels seem to be virtually invisible by the naked eye under daylight due to the inherent high transmittance of the De-SiNCs/DV coating. However, these customized labels can exhibit different patterns with red fluorescence under UV light irradiation at different wavelengths (365 nm and 254 nm), as shown in Fig. 7a. Meanwhile, the printed fabric label with the campus QR code can be quickly recognized as the homepage of Wuhan Textile University by a smartphone, demonstrating exceptional anti-counterfeiting practicability for the De-SiNCs/DV coating.

To further evaluate the anti-counterfeiting performance of the De-SiNCs/DV coating, the "campus QR Codes" are chosen as the evaluation object. As shown in Fig. 7b, the PL emission maximum of the campus QR code is unchangeably centered at around 650 nm as the excitation wavelength increased from 240 nm to 300 nm, implicating the excitation-independent optical property of the De-SiNCs/DV coating. In addition, the fluorescence durability of the anti-counterfeiting coating was also examined by sandpaper. During the rubbing experiment, sandpaper (1200 mesh) was used as an abrasive surface, the representative pattern printed on cotton fabric was placed face down under a 500 g weight on sandpaper and the specimen was dragged in a straight line of 10.4 cm. One back-and-forth movement defines a time period.[45] The fluorescence intensity of the anti-counterfeiting patterns on dry fabric labels gradually decreases with rubbing times. In the meantime, the fluorescence intensity of the wetted campus QR codes on fabric labels also decreases significantly with an increase in the friction time as shown in Fig. 7c. Notably, the dry QR codes printed on cotton fabrics exhibit slightly higher fluorescence intensities as compared to the wetted QR codes on cotton fabrics at the same rubbing times. The lowering fluorescence intensity of the wetted fabric label should be attributable to the enhanced non-radiative decay by absorption of small molecule water after the friction experiment. Overall, the De-SiNCs/DV coating has excellent fluorescence fastness. Moreover, the pH-response to the fluorescence of the campus QR code on the fabric label was also examined to further evaluate the service durability of the De-SiNCs/DV coating. As shown in Fig. 7d, both in acid and alkaline environments, the printed campus QR code on the fabric label still exhibits a high fluorescence intensity, and no change in the PL emission maximum is observed, verifying excellent resistance to acidic and alkaline environments. This excellent acid–base resistance should be attributed to the superior water-repellency of the PDMS composite.

4. Conclusion

In summary, lipophilic De-SiNCs were successfully synthesized by hydrosilylation between H-SiNCs and 1-decene. The morphologies, chemical compositions, stability, and optical properties of the De-SiNCs were characterized. Interestingly, the resultant De-SiNCs are present in a stable mono-dispersed colloid in petroleum ether with a uniform particle size ($\approx$2.9 nm), and exhibit bright red fluorescence under 365 nm light illumination. Subsequently, a new SiNCs/PDMS coating (De-SiNCs/DV) was fabricated by dispersing De-SiNCs into reinforcing PDMS composites with vinyl-capped silicone resin. Interestingly, the De-SiNCs/DV composites exhibit superior transparency (up to 85%) in the visible light range, outstanding fluorescence stabilities with an average lifetime of 20.59 μs under various conditions such as acidic/alkaline solutions, different organic solvents, high-humidity and UV irradiation. Meanwhile, the incorporation of De-SiNCs is beneficial to enhancing the mechanical properties and thermal stability of De-SiNCs/DV composites. Additionally, the De-SiNCs/DV coating exhibits excellent practicability on cotton fabrics when used as an ink in screen-printing. These findings pave the way for exploiting innovative flexible transparent anti-counterfeiting coatings in the future.

Author contributions

Jinfeng Zhang: conceptualization, methodology, data curation, investigation, validation, and writing original draft. Yuanfen Huang: methodology and investigation. Xiaoyuan Zhang: methodology and investigation. Xin Guo: methodology and investigation. Kailong Chen: supervision. Xiang Feng: supervision. Jiajia Kong: supervision. Yanqing Liu: supervision. Bin Shang: supervision. Weilin Xu: supervision. Dongzhi Chen: conceptualization, funding acquisition, supervision, and writing, review and editing.

Data availability statement

The data that support the findings of this study are available from the corresponding author upon reasonable request.

Conflicts of interest

The authors declare no conflicts of interest.

Acknowledgements

This work was supported by the National Natural Science Foundation of China (No. 52173206 and 52203098) and the Applied Foundation Frontier Project from the Wuhan Science and Technology Bureau (No. 2022013988065202). We thank the Analytical and Testing Center of Wuhan Textile University for helps on DMA, NMR and EDS analyses. We also thank Shiyanjia Lab (**www.shiyanjia.com**) for the support of XPS and HRTEM test.

References

1 A. Abdollahi, H. Roghani-Mamaqani, B. Razavi and M. Salami-Kalajahi, *ACS Nano*, 2020, **14**, 14417–14492.
2 H. Suo, Q. Zhu, X. Zhang, B. Chen, J. Chen and F. Wang, *Mater. Today Phys.*, 2021, **21**, 100520.
3 Z. Li, X. Liu, G. Wang, B. Li, H. Chen, H. Li and Y. Zhao, *Nat. Commun.*, 2021, **12**, 1363.
4 J. Xie, X. Sun, X. Guo, X. Feng, K. Chen, X. Shu, C. Wang, W. Sun, Y. Liu, B. Shang, X. Liu, D. Chen, W. Xu and Z. Li, *Carbohydr. Polym.*, 2023, **301**, 120307.
5 Y. Li, C. Chen, M. Jin, J. Xiang, J. Tang, Z. Li, W. Chen, J. Zheng and C. Guo, *Mater. Today Phys.*, 2022, **27**, 100830.
6 F. Zhang, Q. Li, C. Wang, D. Wang, M. Song, Z. Li, X. Xue, G. Zhang and G. Qing, *Adv. Funct. Mater.*, 2022, **32**, 2204487.
7 Z. Luo, Y. Liu, Y. Liu, C. Li, Y. Li, Q. Li, Y. Wei, L. Zhang, B. Xu, X. Chang and Z. Quan, *Adv. Mater.*, 2022, **34**, 2200607.
8 H.-J. Jeon, J. W. Leem, Y. Ji, S. M. Park, J. Park, K.-Y. Kim, S.-W. Kim and Y. L. Kim, *Adv. Funct. Mater.*, 2022, **32**, 2112479.
9 Y. Dong, H. Luan, D. Lin, X. Ma, Z. Wan, B. Li, Q. Zhang, X. Chen, X. Fang and M. Gu, *Laser Photonics Rev.*, 2023, **17**, 2200805.
10 S. Bose, M. A. Ganayee, B. Mondal, A. Baidya, S. Chennu, J. S. Mohanty and T. Pradeep, *ACS Sustainable Chem. Eng.*, 2018, **6**, 6203–6210.
11 Y. Xie, Z. Tong, T. Xia, J. C. Worch, J. Y. Rho, A. P. Dove and R. K. O'Reilly, *Adv. Mater.*, 2024, **36**, 2308154.
12 J. Zhang, R. Tan, Y. Liu, M. Albino, W. Zhang, M. M. Stevens and F. F. Loeffler, *Nat. Commun.*, 2024, **15**, 1040.
13 W. Huang, M. Xu, J. Liu, J. Wang, Y. Zhu, J. Liu, H. Rong and J. Zhang, *Adv. Funct. Mater.*, 2019, **29**, 1808762.
14 X. G. Dongzhi Chen, X. Sun, X. Feng, K. Chen, J. Zhang, Z. Zhu, X. Zhang, X. Liu, M. Liu, L. Li and W. Xu, *Exploration*, 2024, 20230166, DOI: **10.1002/EXP.20230166**.
15 J. Wan, J. Xu, S. Zhu, J. Li and K. Chen, *Chem. Eng. J.*, 2023, **473**, 145500.
16 Y. Liu, W. Chen, L. Lu and B. Yang, *J. Colloid Interface Sci.*, 2022, **609**, 279–288.
17 B. Bai, M. Xu, N. Li, W. Chen, J. Liu, J. Liu, H. Rong, D. Fenske and J. Zhang, *Angew. Chem., Int. Ed.*, 2019, **58**, 4852–4857.
18 T. Lee, B. J. Kim, H. Lee, D. Hahm, W. K. Bae, J. Lim and J. Kwak, *Adv. Mater.*, 2022, **34**, 2106276.
19 T. Subramani, J. Chen, Y.-L. Sun, W. Jevasuwan and N. Fukata, *Nano Energy*, 2017, **35**, 154–160.
20 B. J. Furey, B. J. Stacy, T. Shah, R. M. Barba-Barba, R. Carriles, A. Bernal, B. S. Mendoza, B. A. Korgel and M. C. Downer, *ACS Nano*, 2022, **16**, 6023–6033.
21 R. Shang, F. Yang, G. Gao, Y. Luo, H. You and L. Dong, *Exploration*, 2024, 20230124.
22 R. J. Clark, M. Aghajamali, C. M. Gonzalez, L. Hadidi, M. A. Islam, M. Javadi, M. H. Mobarok, T. K. Purkait, C. J. T. Robidillo, R. Sinelnikov, A. N. Thiessen, J. Washington, H. Yu and J. G. C. Veinot, *Chem. Mater.*, 2017, **29**, 80–89.
23 M. Park, Y. Jeong, H. S. Kim, W. Lee, S.-H. Nam, S. Lee, H. Yoon, J. Kim, S. Yoo and S. Jeon, *Adv. Funct. Mater.*, 2021, **31**, 2102741.
24 J. Sobhanan, J. V. Rival, A. Anas, E. Sidharth Shibu, Y. Takano and V. Biju, *Adv. Drug Delivery Rev.*, 2023, **197**, 114830.
25 D. Chen, W. Sun, C. Qian, A. P. Y. Wong, L. M. Reyes and G. A. Ozin, *Adv. Opt. Mater.*, 2017, **5**, 1700237.
26 X. Guo, X. Sun, J. Zhang, Y. Huang, X. Liu, X. Liu, W. Xu and D. Chen, *Small*, 2023, 2303464.
27 K. Fujimoto, T. Hayakawa, Y. Xu, N. Jingu and K.-I. Saitow, *ACS Sustainable Chem. Eng.*, 2022, **10**, 14451–14463.
28 X. Liu, S. Zhao, W. Gu, Y. Zhang, X. Qiao, Z. Ni, X. Pi and D. Yang, *ACS Appl. Mater. Interfaces*, 2018, **10**, 5959–5966.
29 Y. Xu, S. Terada, Y. Xin, H. Ueda and K.-I. Saitow, *ACS Appl. Nano Mater.*, 2022, **5**, 7787–7797.
30 M. A. Islam, R. Sinelnikov, M. A. Howlader, A. Faramus and J. G. C. Veinot, *Chem. Mater.*, 2018, **30**, 8925–8931.
31 T. Ono, Y. Xu, T. Sakata and K.-I. Saitow, *ACS Appl. Mater. Interfaces*, 2022, **14**, 1373–1388.
32 J. Watanabe, H. Yamada, H.-T. Sun, T. Moronaga, Y. Ishii and N. Shirahata, *ACS Appl. Nano Mater.*, 2021, **4**, 11651–11660.
33 H. Yamada, N. Saitoh, B. Ghosh, Y. Masuda, N. Yoshizawa and N. Shirahata, *J. Phys. Chem. C*, 2020, **124**, 23333–23342.
34 G. Wen, X. Zeng, X. Wen and W. Liao, *J. Appl. Phys.*, 2014, **115**, 164303.
35 M. Sujith, E. K. Vishnu, S. Sappati, M. S. Oliyantakath Hassan, V. Vijayan and K. G. Thomas, *J. Am. Chem. Soc.*, 2022, **144**, 5074–5086.
36 D. Tan, Z. Ma, B. Xu, Y. Dai, G. Ma, M. He, Z. Jin and J. Qiu, *Phys. Chem. Chem. Phys.*, 2011, **13**, 20255–20261.
37 Y. Li, W. Li, H. Zhang, R. Dong, D. Li, Y. Liu, L. Huang and B. Lei, *J. Mater. Chem. B*, 2019, **7**, 1107–1115.
38 S. Shyamsivappan, A. Saravanan, N. Vandana, T. Suresh, S. Suresh, R. Nandhakumar and P. S. Mohan, *ACS Omega*, 2020, **5**, 27245–27253.
39 D. Erb and K. Lu, *Mater. Chem. Phys.*, 2018, **209** 217–226.
40 K. Pan, Z. Zhu, C. Liu, S. Tao, X. Tang, X. Wei and B. Yang, *ACS Appl. Mater. Interfaces*, 2023, **15**, 26060–26068.

41 D. Chen, F. Chen, X. Hu, H. Zhang, X. Yin and Y. Zhou, *Compos. Sci. Technol.*, 2015, **117**, 307–314.
42 S. Tazawa, A. Shimojima, T. Maeda and A. Hotta, *J. Appl. Polym. Sci.*, 2018, **135**, 45419.
43 Y. Han, J. Zhang, L. Shi, S. Qi, J. Cheng and R. Jin, *Polym. Degrad. Stab.*, 2008, **93**, 242–251.
44 Q. Huang, Z. Cai, R. Chen, W. Zhang, D. Nardiello, M. Quinto, X. Liu, S. Hu and T. Sun, *Microchem. J.*, 2022, **183**, 108084.
45 X. Fu, G. Li, S. Cai, H. Yang, K. Lin, M. He, J. Wen, H. Li, Y. Xiong, D. Chen and X. Liu, *Carbohydr. Polym.*, 2021, **251**, 117084.

